



# Heterostructured Er<sup>3+</sup> doped BiVO<sub>4</sub> with exceptional photocatalytic performance by cooperative electronic and luminescence sensitization mechanism

Sergio Obregón, Gerardo Colón\*

Instituto de Ciencia de Materiales de Sevilla, Centro Mixto CSIC-Universidad de Sevilla, C/ Américo Vespucio, 49, 41092 Sevilla, Spain



## ARTICLE INFO

### Article history:

Received 4 March 2014

Received in revised form 8 April 2014

Accepted 15 April 2014

Available online 24 April 2014

### Keywords:

Erbium

BiVO<sub>4</sub>

Photocatalysis

Solar-like

O<sub>2</sub> evolution

## ABSTRACT

Er-BiVO<sub>4</sub> has been synthesized by means of mw-assisted hydrothermal method having good photoactivity under sun-like excitation. It is stated that the precursor addition sequence plays a critical role which determine the further structural feature of BiVO<sub>4</sub>. From the structural and morphological characterization, it can be demonstrated that the presence of Er<sup>3+</sup> would induce the stabilization of the tetragonal phase probably due to the formation of tetragonal-ErVO<sub>4</sub> seeds previous to BiVO<sub>4</sub> formation. The best photocatalytic performance is attained for the sample with 0.75 at% Er<sup>3+</sup> content. At this dopant loading a mixture of tetragonal and monoclinic phase (70% tetragonal) is obtained. The dramatic increase in the photocatalytic activity for 0.75 at% Er-BiVO<sub>4</sub> is related to the occurrence of such heterostructure. For this system, the MB degradation rate constant appears drastically higher as bare m-BiVO<sub>4</sub>. Furthermore, activities of photocatalysts for visible-light-driven O<sub>2</sub> evolution have been evaluated, demonstrating that the photocatalytic activity of this Er-doped system (O<sub>2</sub> evolution rate, 1014 μmol g<sup>-1</sup> h<sup>-1</sup>) is 20 times as that of undoped m-BiVO<sub>4</sub> (O<sub>2</sub> evolution rate, 54 μmol g<sup>-1</sup> h<sup>-1</sup>). From the obtained results, the cooperative conjunction of electronic and luminescence mechanism involved in the reaction is proposed to be the origin of the enhanced photocatalytic efficiencies of such systems.

© 2014 Elsevier B.V. All rights reserved.

## 1. Introduction

During the last decades, the efficient utilization of solar light has been largely pursued. For this scope several tactics have been established for enhancing the spectral response of photocatalysts. For this scope, the recent research activity in the field of the heterogeneous photocatalysis has been focused in the development of novel alternative materials to traditional TiO<sub>2</sub> capable to use of sunlight as green energy source [1]. Recently, the visible-light-active BiVO<sub>4</sub> has become worthy of consideration as an advanced material for photocatalytic applications, used as well as in water splitting, CO<sub>2</sub> reduction and organic contaminants decomposition under visible-light irradiation [2–6]. It has been widely reported that the photocatalytic properties of BiVO<sub>4</sub> are strongly dependent on its structure and morphology [6–10]. According to previous reports, BiVO<sub>4</sub> appears in three main crystalline phases: monoclinic scheelite, tetragonal zircon, and tetragonal scheelite [11,12].

From this extensive literature, the photocatalytic activity for different BiVO<sub>4</sub> phases arises quite different. Thus, monoclinic BiVO<sub>4</sub> (m-BiVO<sub>4</sub>) gives the best visible-light-driven photocatalytic performance, while the photoactivity of tetragonal BiVO<sub>4</sub> (t-BiVO<sub>4</sub>) appears almost negligible [13–15]. One of the claimed reason is that the band gap values of t-BiVO<sub>4</sub> and m-BiVO<sub>4</sub> are quite different (2.9 and 2.4 eV respectively). From this band structure, the t-BiVO<sub>4</sub> mainly possesses a UV absorption band, while m-BiVO<sub>4</sub> has a characteristic visible light absorption band besides the UV band. The origin of such higher visible photoactivity of m-BiVO<sub>4</sub> lies on the transition from a valence band formed by Bi 6s or a hybrid orbital of Bi 6s and O 2p to a conduction band of V 3d and its narrower band gap [16]. Furthermore, from DFT calculations it has been stated that the mobility difference of hole along both structures may provide an explanation for the enhanced photocatalytic activity of m-BiVO<sub>4</sub> over t-BiVO<sub>4</sub> [17]. However, pristine m-BiVO<sub>4</sub> still shows a scarce photocatalytic activity owing to poor charge-transport characteristics and the weak surface adsorption properties [18,19].

In order to improve the photocatalytic activity of m-BiVO<sub>4</sub>, different approaches have been proposed including heterojunction structure formation [18,20,21], co-catalysts loading [22,23],

\* Corresponding author. Tel.: +34 954489536; fax: +34 954460665.

E-mail address: [gcolón@icmse.csic.es](mailto:gcolón@icmse.csic.es) (G. Colón).

and impurity doping [24,25]. Among these approaches, the co-existence of monoclinic–tetragonal heterostructure appears as a new way to be considered. Recently, Tan et al. demonstrated that the existence of a mixed-phase  $\text{BiVO}_4$  showed higher photocatalytic activity [26]. Similarly, Fan et al. reported that the particular m–t heterostructured  $\text{BiVO}_4$  is expected to promote the separation of photoinduced electron–hole pairs [27]. Within this framework, we have recently reported the preparation of heterostructured monoclinic–tetragonal  $\text{BiVO}_4$  by means of yttrium doping with improved photocatalytic activity [28]. The occurrence of a heterostructured material clearly leads to an improved charge carrier separation and therefore to a lower recombination process.

Among lanthanides,  $\text{Er}^{3+}$  constitutes an interesting option to be considered for tetragonal stabilization. Furthermore, it is widely reported that Er exhibits interesting luminescence properties. This fact makes erbium doping an interesting approach since as up-converting nanomaterials could be excited by visible-light or NIR, showing luminescence in the visible and ultraviolet [29]. Recently, we have demonstrated the assembly of  $\text{TiO}_2$  with such up-converting doping cation showing a double mechanism, under UV and NIR excitation [30]. Within this configuration the improvement is reached by light engineering. The increasing of the number of incoming radiation photons absorbed by the photocatalyst is achieved by wavelength conversion material [31]. Considering an up-converting luminescent material, it would absorb low energy radiation (i.e. on the NIR or visible range) and emit higher energy radiation (i.e. in the visible and/or UV). Recently, Tang et al. reported a core-shell structured nanoparticles for near-infrared (NIR) photocatalysis. In this complex structure, the core is composed of up-conversion luminescence  $\text{NaYF}_4\text{:Yb,Tm}$  and the shell is anatase  $\text{TiO}_2$  nanocrystals around  $\text{NaYF}_4$  particles [32]. Within a similar approach, it has been demonstrated that the  $\text{YF}_3\text{:Yb,Tm@TiO}_2$  structures exhibit interesting photocatalytic activities under the irradiation of both UV and near IR light [33,34]. Within this framework, we presented in a previous paper the unexpected enhanced photocatalytic activity of tetragonal stabilized Er-doped  $\text{BiVO}_4$  prepared by microwave assisted hydrothermal method [35]. On this basis, in the present paper we show the preparation of a monoclinic–tetragonal heterostructured  $\text{Er}^{3+}$ - $\text{BiVO}_4$  exhibiting a notably high photoactivity under sun-like irradiation. Thus, by choosing the adequate synthetic strategy we are able to obtain a mixed phase heterostructure with a drastically higher photocatalytic activity.

## 2. Experimental

### 2.1. $\text{Er}^{3+}$ - $\text{BiVO}_4$ heterostructure preparation

The preparation of  $\text{Er}^{3+}$  doped  $\text{BiVO}_4$ , has been followed by a modified method previously reported [35]. As it can be stated from the obtained results, such modification will remarkably affect to the final structural and photocatalytic performance of the obtained materials. Firstly, 5 mmol of  $\text{Bi}(\text{NO}_3)_3 \cdot 5\text{H}_2\text{O}$  was dissolved in 10 mL of glacial acetic acid at room temperature. A second aqueous solution was prepared by dissolving the corresponding stoichiometric amount of  $\text{NH}_4\text{VO}_3$  and the stoichiometric amount of  $\text{Er}(\text{NO}_3)_3$  (from 0.25 to 4.0 at% with respect to  $\text{BiVO}_4$ ) in 60 mL of hot distilled water. A milky colloidal suspension is formed, probably due to the formation of small  $\text{ErVO}_4$  seeds. Afterwards, the ammonium metavanadate solution was added to the bismuth nitrate aqueous solution and the process was accompanied with a vigorous stirring. The pH of the obtained suspension was adjusted to 9.0 by adding concentrated  $\text{NH}_4\text{OH}$  ( $13 \text{ mol L}^{-1}$ ). The slurry was encased in a Teflon vessel and heated under microwave irradiation using a microwave reactor (model MWO-1000S, Eyela; Japan). The

temperature was fixed at  $140^\circ\text{C}$  with a maximum variable power of 195 W during 30 min. The obtained precipitate was then cooled until room temperature, filtered and repeatedly washed and dried overnight at  $120^\circ\text{C}$ . Afterwards, thus obtained samples were submitted to a further calcination treatment at  $300^\circ\text{C}$  for 2 h.

### 2.2. Materials characterization

BET surface area and porosity measurements were carried out by  $\text{N}_2$  adsorption at  $-196^\circ\text{C}$  using a Micromeritics 2010 instrument. X-ray diffraction (XRD) patterns were obtained using a Siemens D-501 diffractometer with Ni filter and graphite monochromator. The X-ray source was  $\text{Cu K}\alpha$  radiation ( $0.15406 \text{ nm}$ ). Rietveld analyses were performed by using XPert HighScore Plus software over selected samples. The diffraction patterns were recorded from  $2\theta$   $10^\circ$  to  $120^\circ$  with step of  $0.017^\circ$  and 400 s per step. Crystallite sizes were obtained from Rietveld refinement. Micro-Raman measurements were performed using a LabRAM Jobin Yvon spectrometer equipped with a microscope. Laser radiation ( $\lambda = 532$  and  $780 \text{ nm}$ ) was used as excitation source at 5 mW. All measurements were recorded under the same conditions (2 s of integration time and 30 accumulations) using a  $100\times$  magnification objective and a 125 mm pinhole. The morphology of samples was followed by means of field emission-SEM (Hitachi S 4800). The samples were dispersed in ethanol using an ultrasonicator and dropped on a copper grid.

The UV diffuse reflectance spectra were measured using an UV-vis spectrophotometer equipped with an integrating sphere (JASCO V-570). The reference sample used was a  $\text{BaSO}_4$  coated standard pattern. The photoluminescence emission spectra of the powdered pressed catalysts were recorded at ambient temperature in a Horiba Jobin-Yvon Fluorolog3 spectrofluorometer operating in the front face mode.

### 2.3. Photocatalytic tests

The photocatalytic activity of the samples was tested by means the degradation of Methylene Blue dye (MB) under simulated solar conditions. In a typical procedure, 0.05 g of photocatalyst was placed in a batch reactor containing 50 mL of MB whose initial concentration was  $10 \text{ mg L}^{-1}$ . The suspension was maintained under dark conditions for 15 min in order to achieve the adsorption–desorption equilibrium of the dye on the photocatalyst surface. Afterwards, the suspension was irradiated with simulated solar light by means a solar simulator PEC-L01, Peccell equipped with a 150 W Xe lamp ( $150 \text{ W cm}^{-2}$ , 1.5 sun). Samples of 1 mL were taken at given interval times and the photocatalyst was separated using a nylon filter. The concentrations were monitored by checking the absorption spectrum of each sample through its absorption band maximum (664 nm) using an UV-Vis spectrophotometer (Mecasys Optizen 2120UV). The photocatalytic activities of the samples were also evaluated for the photocatalytic oxygen evolution reaction from water in an  $\text{AgNO}_3$  aqueous solution (0.02 M). The reaction media was continuously thermostated at  $23\text{--}25^\circ\text{C}$  to prevent any significant evaporation of the sacrificial agent. The catalyst suspension ( $1 \text{ g L}^{-1}$ ) was firstly degassed with an  $\text{N}_2$  stream ( $150 \text{ mL min}^{-1}$ ) for 30 min. After that the  $\text{N}_2$  flow was settled at  $15 \text{ mL min}^{-1}$  and stabilized for 15 min. This nitrogen flow was used to displace the oxygen produced from the photoreactor headspace toward the GC measuring system. Then, the lamp (200 W Hg-Xe lamp, Oriel Instruments) was switched on and the effluent gases were analyzed to quantify  $\text{O}_2$  production by gas chromatography (Agilent 490 micro GC) using a thermal conductivity detector connected to a Molsieve 5 A column.

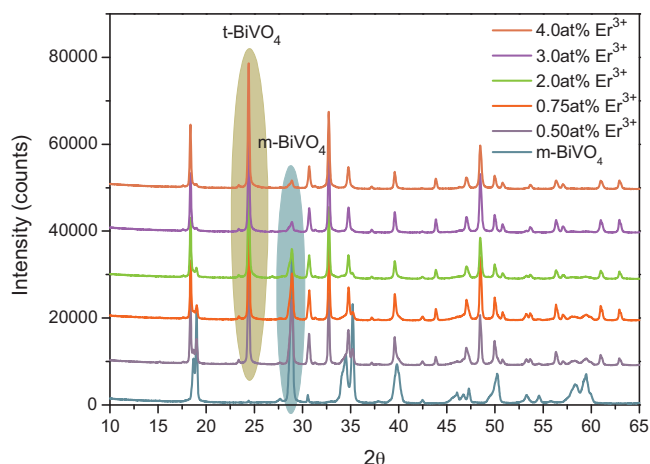


Fig. 1. X-ray diffraction patterns for Er-BiVO<sub>4</sub> catalysts obtained by mw-hydrothermal synthesis at 140 °C for 30 min.

### 3. Results and discussion

#### 3.1. Results description

As can be noticed from the XRD pattern, doped BiVO<sub>4</sub> shows a mixture of monoclinic (PDF 75-1866) and tetragonal (PDF 14-0133) crystalline phases. It is clear that the presence of Er<sup>3+</sup> cation strongly stabilizes tetragonal phase of BiVO<sub>4</sub>. Thus, the tetragonal structure is noticeable just from the lowest content of dopant, being in all cases the predominant one (Fig. 1). Tetragonal fraction calculated from Rietveld analysis clearly increases as erbium loading grows up reaching the maximum value for 5.0 at% of Er<sup>3+</sup> for which only the tetragonal phase is present (Fig. 2). The observed evolution of the crystalline structure of Er-doped BiVO<sub>4</sub> systems with Er<sup>3+</sup> content is significantly different from that previously reported, for which the tetragonal phase was predominant for Er<sup>3+</sup>

content above 3 at% [35]. It is clear that the change in the precursor addition drastically conditions the stabilization of the tetragonal phase even at lowest erbium contents.

Moreover, by observing the evolution of the cell features obtained from Rietveld refinement with erbium content, it is worthy to note that in this case erbium incorporation is taking place in a different way. Thus, the monoclinic cell volume seems to be more affected than in the previous reported one (Fig. 2). Furthermore, the tetragonal cell volume although exhibits a certain contraction tendency, the observed decrease is weaker. From these results, it appears that Er<sup>3+</sup> is located preferentially in the monoclinic phase, causing a notably expansion of the cell.

As its cell volume rises, it might be assumed that Er<sup>3+</sup> ions are located interstitially. Thus, for this preparation sequence erbium is placed in both structures from the lowest content, being more important the observed distortion for the monoclinic phase. By

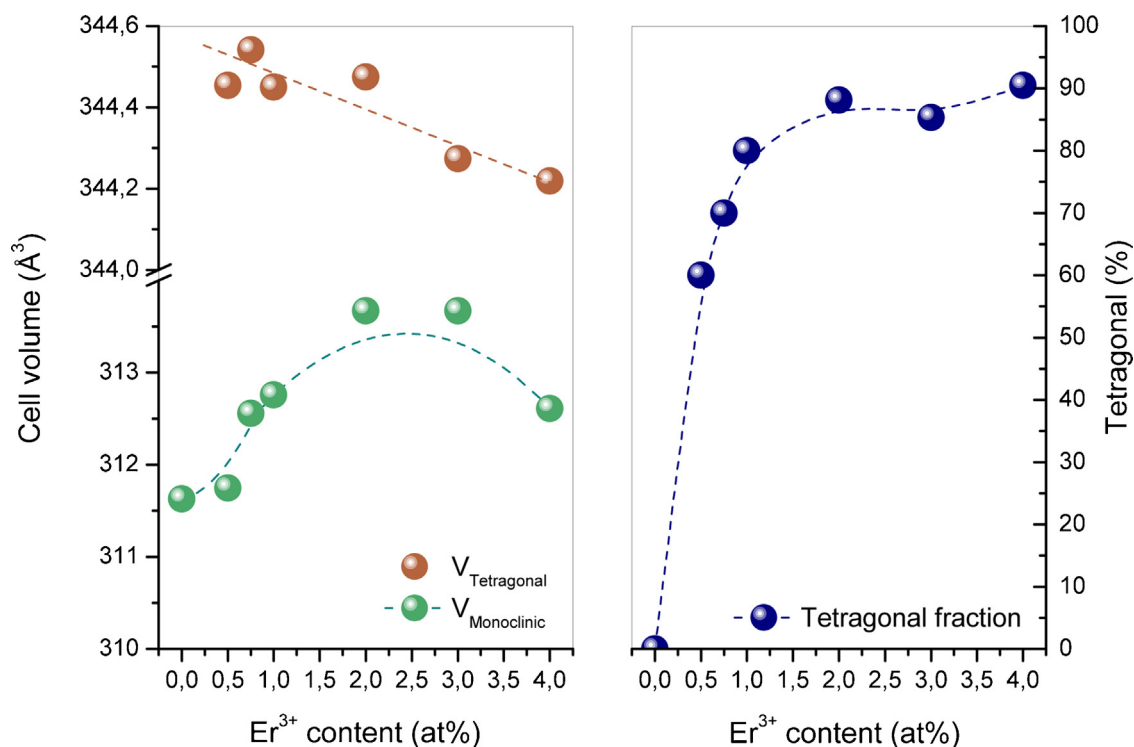
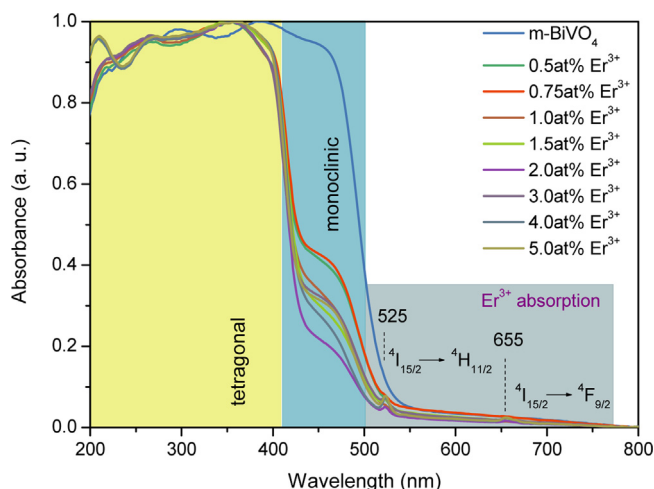


Fig. 2. Evolution of the cell volume and the tetragonal phase fraction with Er<sup>3+</sup> content. Evolution of cell parameters for monoclinic and tetragonal crystalline phase for Er-BiVO<sub>4</sub> series.

**Table 1**Structural parameters, surface area values and O<sub>2</sub> evolution reaction rates for Er<sup>3+</sup> doped BiVO<sub>4</sub> catalysts.

Samples	Monoclinic			Tetragonal			BET (m <sup>2</sup> /g)	O <sub>2</sub> evolution reaction rate (mmol g <sup>-1</sup> h <sup>-1</sup> )
	<i>a</i>	<i>b</i>	<i>c</i>	$\beta$	<i>a</i> = <i>b</i>	<i>c</i>		
BiVO <sub>4</sub>	5.2115	5.1022	11.7198	90.42	–	–	1	54
Er-BiVO <sub>4</sub> 0.50 at%	5.2157	5.1052	11.7082	90.45	7.3021	6.4591	3	522
Er-BiVO <sub>4</sub> 0.75 at%	5.2224	5.1086	11.7157	90.49	7.3029	6.4602	3	1014
Er-BiVO <sub>4</sub> 1.0 at%	5.2264	5.1088	11.7141	90.52	7.3023	6.4596	5	692
Er-BiVO <sub>4</sub> 1.5 at%	–	–	–	–	–	–	5	629
Er-BiVO <sub>4</sub> 2.0 at%	5.2341	5.1169	11.7123	90.57	7.3025	6.4597	5	603
Er-BiVO <sub>4</sub> 3.0 at%	5.2400	5.1128	11.7086	90.63	7.3011	6.4584	7	592
Er-BiVO <sub>4</sub> 4.0 at%	5.2204	5.1312	11.6705	90.23	7.3005	6.4584	6	539
Er-BiVO <sub>4</sub> 5.0 at%	–	–	–	–	–	–	7	540

**Fig. 3.** Diffuse reflectance UV-vis spectra for Er-BiVO<sub>4</sub> series.

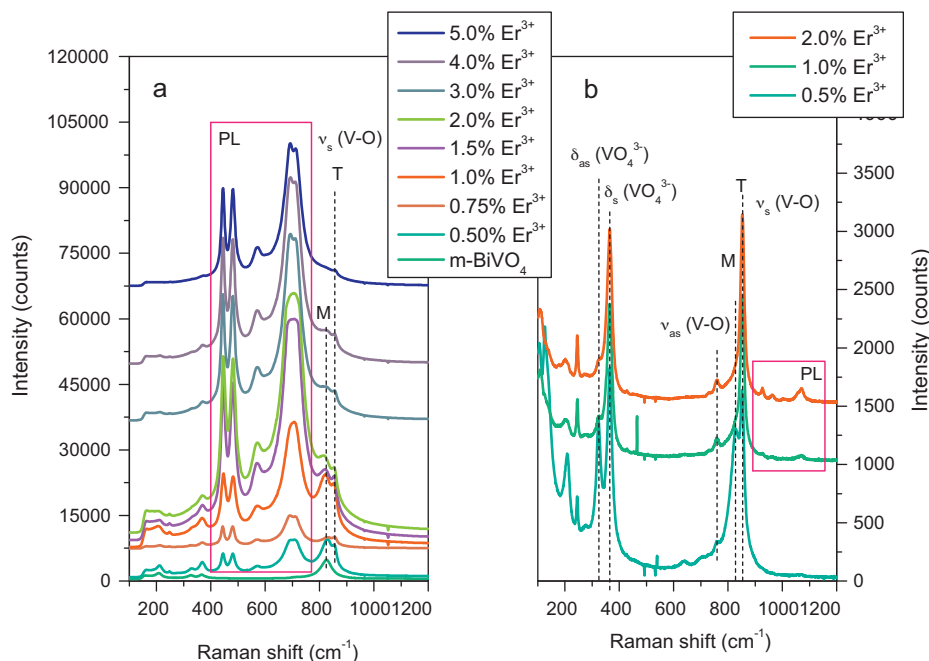
following the cell parameters it might be said that the monoclinic cell enlargement is caused by the elongation of *a* and *b* parameters, while *c* parameter suffers a slight shrinkage (Table 1). For the tetragonal structure, both *a* = *b* and *c* parameters show a slight diminution which is the reason of the cell volume decrease. Thus,

attending to the ionic radii for Bi<sup>3+</sup> and Er<sup>3+</sup>, it is expected that erbium cation would occupy the bismuth position in the tetragonal cell producing the observed cell contraction.

In accordance with literature, the surface area obtained for all samples are significantly low (Table 1). However, systems with certain fraction of the tetragonal phase show slight increase in surface area.

From diffuse reflectance spectra, two clear absorption edges can be noticed when tetragonal phase is present (Fig. 3). The calculated band gap values at  $2.4 \pm 0.1$  and  $2.8 \pm 0.1$  eV from these two absorption edges would be associated to the monoclinic and tetragonal phases respectively, which are in accordance with those reported in the literature [15]. Additionally to the BiVO<sub>4</sub> absorption, two minor bands can be found at 525 and 655 nm. Such bands can be associated to the presence of Er<sup>3+</sup> and would correspond to the transition from the <sup>4</sup>I<sub>15/2</sub> ground state to the <sup>4</sup>H<sub>11/2</sub> and <sup>4</sup>F<sub>9/2</sub> excited states respectively [36].

In Fig. 4, we report the Raman spectra corresponding to the Er<sup>3+</sup>-BiVO<sub>4</sub> samples. Raman bands around 158, 208, 324, 362, 710, and 826 cm<sup>-1</sup> were observed for bare BiVO<sub>4</sub>, which are typical vibrational bands of m-BiVO<sub>4</sub> [12,37,38]. As erbium is present, strong luminescence bands corresponding to the fluorescence emission of Er<sup>3+</sup> upon green laser excitation (532 nm) are also detected (Fig. 4a). Additionally, it is also worthy to note the appearance of a new shoulder at 850 cm<sup>-1</sup> which corresponds to V–O symmetric

**Fig. 4.** Raman spectra for Er-BiVO<sub>4</sub> series under (a) green laser excitation (532 nm); (b) red laser (780 nm) excitation.

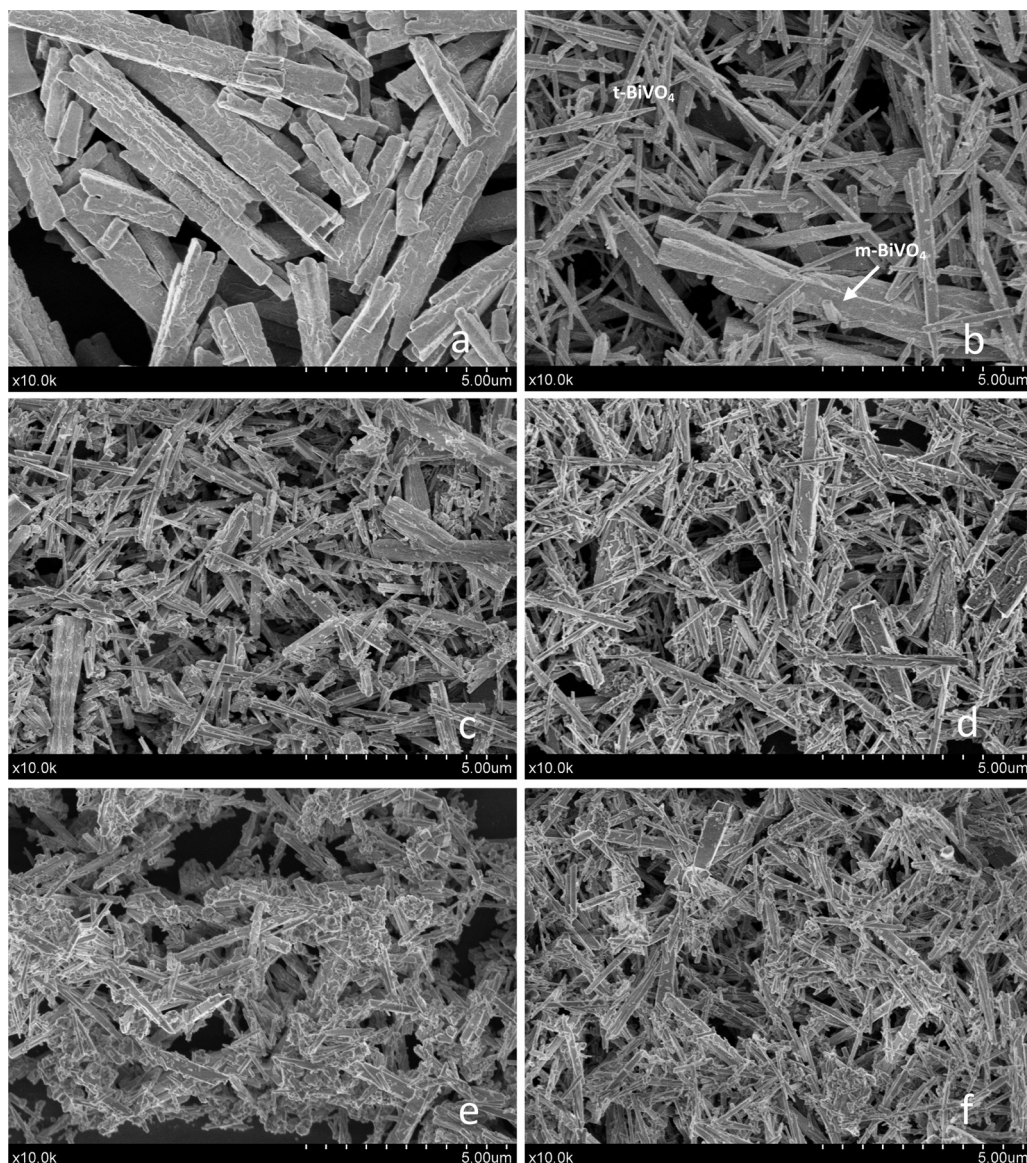


**Fig. 5.** Selected FESEM images for Er-BiVO<sub>4</sub> series with different erbium content: (a) bare BiVO<sub>4</sub>, (b) 0.5 at%, (c) 0.75 at%, (d) 2.0 at%, (e) 3.0 at% and (f) 4.0 at% of Er<sup>3+</sup>.

stretching mode for t-BiVO<sub>4</sub> structure. The Raman spectra registered upon red laser excitation (Fig. 4b) clearly shows only the Raman bands associated to m-BiVO<sub>4</sub> and t-BiVO<sub>4</sub> since no luminescence is present.

Thus, the occurrence of such luminescence process might be associated to the presence of the tetragonal structure along the whole series. In addition, the appearance of a noticeable shoulder at around 850 cm<sup>-1</sup> corresponding to the symmetric V–O stretching mode points out the coexistence of the monoclinic and tetragonal structures [12]. This mixture is more evidenced from the Raman spectra obtained upon red laser excitation for which luminescence is almost suppressed (Fig. 4b).

The morphology of BiVO<sub>4</sub> has extensively reported to be dependent on the preparation route [39,40]. In our case, bare BiVO<sub>4</sub> shows a square rod-like morphology (Fig. 5a). Such morphology leads to the partial extinction of the (040) diffraction line and the notably exaltation of diffraction lines corresponding to the planes (110) and (002), as was observed in the XRD pattern (Fig. 1). The morphology of Er-doped systems clearly denotes the structural mixture (Fig. 5b). Thus, for the whole series, both morphologies (square rods and needle-like particles) cohabit from the lowest

Er<sup>3+</sup> content. As dopant loading increases, the shapes of acicular particles seems be partially destroyed and other small particles progressively appear (Fig. 5e and f).

In order to understand the role of erbium doping in the luminescence properties of our catalysts, we have performed the photoluminescence spectra upon 523 and 655 nm excitation, at which Er<sup>3+</sup> showed characteristic absorption bands (Fig. 6).

The emission spectra upon 523 nm excitation clearly exhibit two clear bands at 492 and 505 nm. The intensity of such bands gradually increases as erbium content increases. This growing intensity could be related with the progressive appearance of the tetragonal structure. Thus, the occurrence of this later phase is closely related to the presence of the luminescence properties of the system. This result is in accordance with the evolution of luminescence in Raman spectra (Fig. 4a). It can be also noticed that the intensity of the luminescence is remarkably lower than that obtained in our previous series [35]. This fact could be related with the existence of the m-BiVO<sub>4</sub> in a higher fraction. Upon 655 nm excitation, notably poor bands are observed in the 400–600 nm range. Worth noting is the fact that while 1.5 at% and 4.0 at% photocatalysts show similar emission bands in that range, for 0.75 at% the up-converted emission is

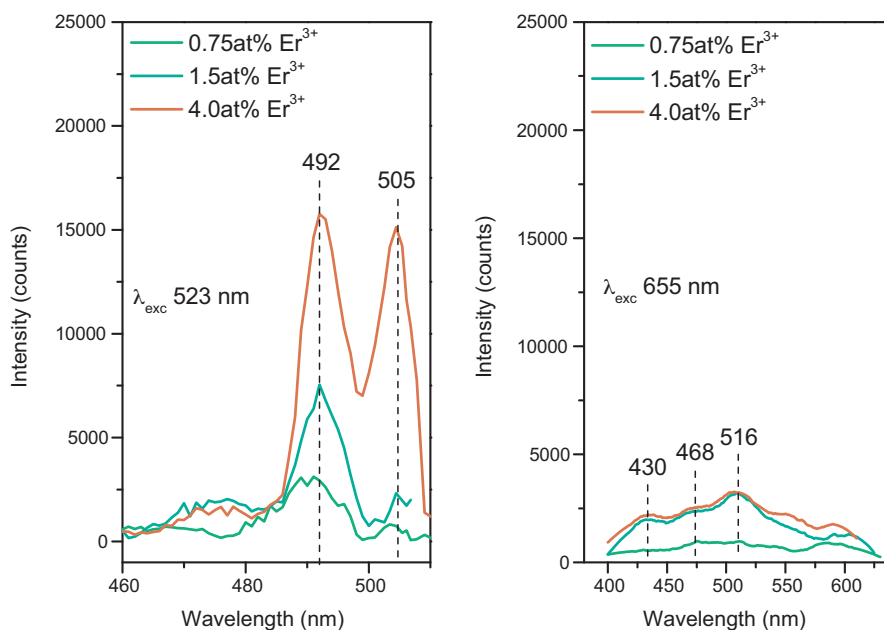


Fig. 6. PL spectra for Er-BiVO<sub>4</sub> series upon 523 and 655 nm excitation.

almost suppressed. It has been reported that violet (405–420 nm), blue (436–442 nm) and green (525–575 nm) up-conversion luminescence were simultaneously observed upon excitation at 652 nm [41–43]. Thus, the absence of such bands would be associated to the efficiently absorption by m-BiVO<sub>4</sub> and t-BiVO<sub>4</sub> matrix.

It is worthy to note that the preparation of BiVO<sub>4</sub> by mw-assisted hydrothermal method leads to higher photoactivity with respect to that prepared by simple coprecipitation method (Fig. 7). For doped heterostructured BiVO<sub>4</sub> photocatalysts, the photocatalytic performance shows a dramatic improvement with respect to bare BiVO<sub>4</sub> and even for previously reported Er<sup>3+</sup>-BiVO<sub>4</sub> system (Fig. 7) [35]. The optimum conversion value is achieved by 0.75 at% of erbium content. For this doping level, the complete MB

degradation is achieved before 40 min of illumination. In spite that a direct comparison is difficult and might take into consideration the operational parameters, this result clearly overcomes other published result obtained under similar conditions [26,27,44,45]. Moreover, the reaction rate for this catalyst is ca. 6 times higher than the best value obtained for previous series (Er<sup>3+</sup>-BiVO<sub>4</sub> 4.0 at%) and 20 times higher than that for bare BiVO<sub>4</sub>!!

We have to remark that in all cases, the tetragonal phase is the main one. However, higher monoclinic fraction is present in this series with respect to the systems previously reported by us.

Furthermore, in Fig. 8 it is shown the photocatalytic water oxidation activity of different Er<sup>3+</sup>-doped BiVO<sub>4</sub> samples from an aqueous solution containing AgNO<sub>3</sub> as a sacrificial reagent under

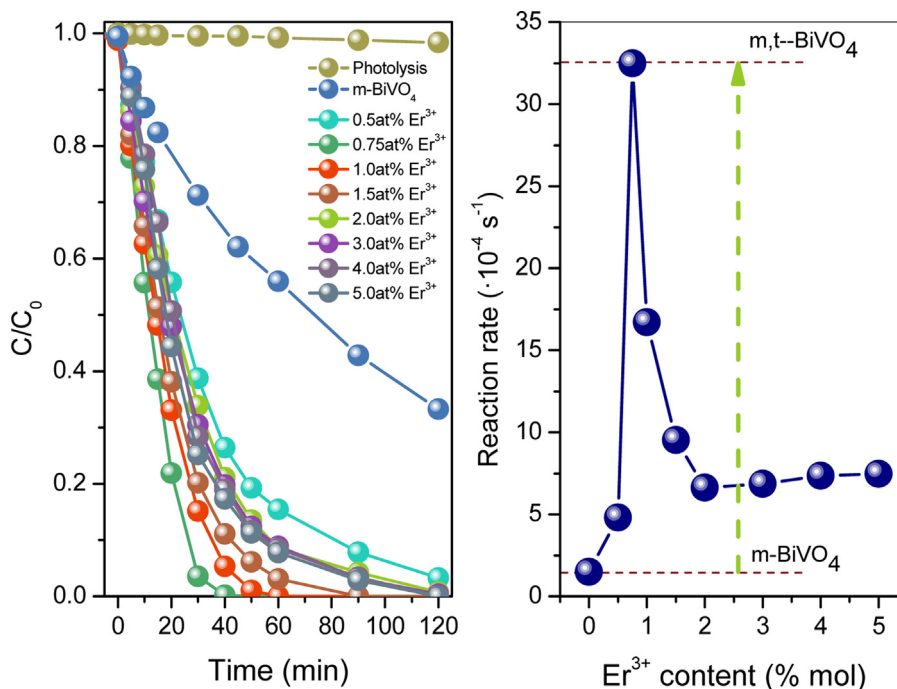
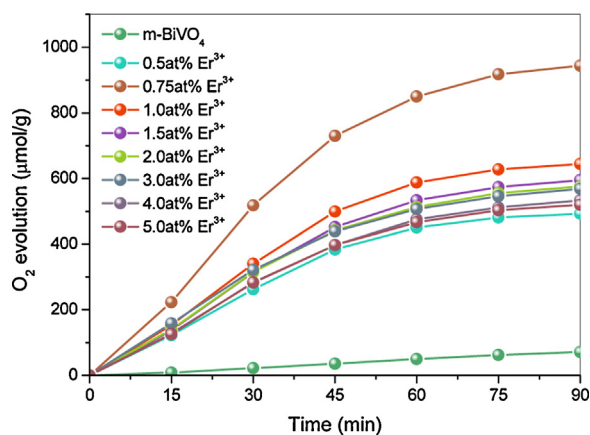


Fig. 7. Photocatalytic degradation of MB and reaction rates for Er-BiVO<sub>4</sub> series.



**Fig. 8.** Photocatalytic  $\text{O}_2$  evolution of the samples from aqueous  $\text{AgNO}_3$  solutions ( $0.02 \text{ mol L}^{-1}$ ) for  $\text{Er}^{3+}$ - $\text{BiVO}_4$  systems as a function of the irradiation time.

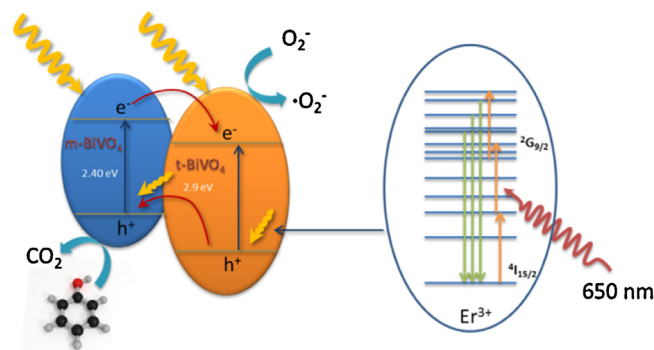
sunlight irradiation. As  $\text{Er}^{3+}$  is incorporated the photoactivity for  $\text{O}_2$  rapidly increases (Table 1), reaching a maximum  $\text{O}_2$  evolution rate for 0.75 at% doped sample ( $1014 \mu\text{mol h}^{-1} \text{ g}^{-1}$ ). Such value is about 20 times of that of bare  $\text{BiVO}_4$  ( $54 \mu\text{mol h}^{-1} \text{ g}^{-1}$ ) and appears also notably if compared to best reported in the literature [45,46].

So, for this reaction the optimum performance observed for 0.75 at% catalysts is maintained with respect to bare m- $\text{BiVO}_4$ .

### 3.2. Discussion of the results

By modifying the synthetic route, we have obtained an  $\text{Er}^{3+}$ -doped  $\text{BiVO}_4$  series with significantly different structural and optical behavior and a dramatic enhanced photoactivity. The structural features and their evolutions with erbium content clearly point out a key role of precursor addition sequence. Thus, while for  $\text{Er}^{3+}$ - $\text{Bi}^{3+}$  precursors joint addition the main crystalline phase is the monoclinic one, which develops toward tetragonal for high  $\text{Er}^{3+}$  content, for  $\text{Er}^{3+}$ - $\text{V}^{5+}$  precursors joint addition sequence series the tetragonal phase appears just from the lowest dopant content. The fast precipitation of  $\text{BiVO}_4$  when vanadate is added to  $\text{Bi}^{3+}$  solution would suggest that  $\text{Er}^{3+}$  is not effectively enclosed in the structure, occupying interstitial sites. Thus, only when erbium content is present at high concentration the tetragonal phase is favored and  $\text{Er}^{3+}$  ions occupy the  $\text{Bi}^{3+}$  sites [35]. By changing the addition sequence,  $\text{Er}^{3+}$  is added to vanadate previously, it could be assumed that t- $\text{ErVO}_4$  small seeds could be formed which clearly condition the topotactically formation of  $\text{BiVO}_4$  in the tetragonal form (Fig. 4). The observed cell distortion clearly points out that upon  $\text{Bi}^{3+}$  addition progressive cation diffusion is taking place leading to the formation of  $\text{Er}^{3+}$ -doped  $\text{BiVO}_4$  system. Thus, t- $\text{BiVO}_4$  is present just from the lowest  $\text{Er}^{3+}$  content. At the same time, certain Er,Bi-vanadate species could also be formed which would progress toward the monoclinic structure, keeping  $\text{Er}^{3+}$  ions interstitially in great extent with respect t- $\text{BiVO}_4$ .

The structural behavior of both series depending on addition sequence is also accompanied by the exaltation of the luminescence properties of the rare earth cation (Fig. 4). Thus, only when  $\text{Er}^{3+}$  occupies the  $\text{Bi}^{3+}$  sites in the t- $\text{BiVO}_4$  structure visible luminescence is noticed. From photoluminescence spectroscopy we have stated that clear emission bands are detected at 492 and 505 nm. The energy of these emitted photons clearly fit with the absorption edge of m- $\text{BiVO}_4$ . Therefore, it would be expected that m- $\text{BiVO}_4$  would have certain extra photons available from luminescence process. In addition, the lack of emission bands in the range 400–600 nm upon 655 nm excitation would also indicate the effectively absorption by m- $\text{BiVO}_4$  and t- $\text{BiVO}_4$ .



**Scheme 1.** Envisaged electronic scheme involved in the photocatalytic mechanism upon solar-like excitation.

By considering the above structural and luminescence properties, it is possible envisage the complex cooperative mechanism involved in the overall process. When  $\text{Er}^{3+}$  is doping the monoclinic phase we could explain the observed improvement in terms of classical doping theory in which dopant would help to the charge separation till its concentration is detrimental and promote the recombination process [47]. Thus, in our previous paper we could notice the slight increase in the reaction rate for m- $\text{BiVO}_4$  till  $\text{Er}^{3+}$  content was 2.0 at%, for which no luminescence emission was observed [35]. Therefore, Er-doped monoclinic structure a more effective charge separation can be the responsible of the photocatalytic activity.

The photocatalytic behavior of the present studied system is completely different, clearly showing a drastic enhancement with respect the previously reported series. The maximum photoactivity is achieved for 0.75 at%  $\text{Er}^{3+}$  doping. For this sample for which a mixture of tetragonal and monoclinic is present, a strong photoluminescence is observed. Therefore, the tight interface junction formed between the m- $\text{BiVO}_4$  and t- $\text{BiVO}_4$  and the existence of an up-conversion mechanism would be the responsible of the significantly enhanced photoactivity. From this scheme, t- $\text{BiVO}_4$  would act as internal sensitizer for m- $\text{BiVO}_4$  providing extra photons with the adequate energy (Scheme 1). In addition to this supportive double mechanism, the formation of a mixed phase structure is of great importance. As reported by Fan et al., the particular heterostructured  $\text{BiVO}_4$  is expected to promote the separation of photoinduced electron-hole pairs [27]. Moreover, and as it has been previously observed, Er-doping would also affect to the efficiency of charge separation. Thus, the enhanced photoactivity would be achieved by both, increasing of the appropriate photons as well as by the optimization of the electron-hole separation in the double way we stated.

### 4. Conclusions

By the appropriate control of the synthetic parameters, especially the precursor addition sequence, we have obtained a significantly high photoactive Er- $\text{BiVO}_4$  system. Thus, the occurrence of a tetragonal-monoclinic heterostructured material, together with a cooperative up-conversion process might be the origin of this exalted photoactivity. The optimum reaction rate obtained for 0.75 at% Er-doped  $\text{BiVO}_4$  (70% of tetragonal phase) for MB degradation reaction is 20 times higher than that attained for bare  $\text{BiVO}_4$ !! Moreover, the  $\text{O}_2$  evolution reaction rate for photocatalyst is drastically higher with respect to undoped m- $\text{BiVO}_4$ . This result clearly overcomes all reported data for t- $\text{BiVO}_4$ .

The stabilization of the tetragonal phase is directly related with the presence of  $\text{Er}^{3+}$  doping ions which trends to substitute  $\text{Bi}^{3+}$  within this crystalline phase. We have stated that such stabilization

is strongly affected by the sequence of precursor addition. Thus, a great difference in the structural feature of the systems from series obtained by  $\text{Er}^{3+}$ – $\text{V}^{5+}$  precursors joint addition sequence is noticed. The formation of  $\text{ErVO}_4$  seeds previously to the addition of  $\text{Bi}^{3+}$  within the proposed preparation route could be the reason of the tetragonal stabilization.

Once the tetragonal phase appears, the  $\text{Er}^{3+}$ – $\text{BiVO}_4$  systems exhibit strong luminescence behavior. Therefore, the dramatic improve in the photocatalytic activity shown by the  $\text{Er}^{3+}$ – $\text{BiVO}_4$  could be correlated to a cooperative process involving the electronic and luminescence mechanism. As tetragonal phase is present, a double mechanism could be envisaged. Firstly, the contribution of extra-photons generated by luminescence process in the overall mechanism due an energy transfer process from erbium ions to t- $\text{BiVO}_4$  and m- $\text{BiVO}_4$  could be proposed. This sensitization mechanism will indeed improve the photon efficiency of the photocatalytic process. Secondly, and not less important, the formation of a monoclinic–tetragonal heterostructure could be also the responsible of a more effective charge separation.

### Acknowledgments

This work was supported by Spanish MINECO and Junta de Andalucía (ENE2011-24412 and P09-FQM-4570 projects). S. Obregón thanks CSIC for the concession of a JAE-Pre grant. Authors also thank Dr. A.I. Becerro for Rietveld refinement. Author thanks the Global Research Laboratory Program of the National Foundation of Korea funded by the Ministry of Education, Science and Technology of South Korea (Grant Number: 2010-00339).

### References

- [1] A. Kubacka, M. Fernández-García, G. Colón, *Chem. Rev.* 112 (2012) 1555.
- [2] A. Kudo, K. Omori, H. Kato, *J. Am. Chem. Soc.* 121 (1999) 11459.
- [3] J. Yu, A. Kudo, *Adv. Funct. Mater.* 16 (2006) 2163.
- [4] Y. Sasaki, A. Iwase, K. Kato, A. Kudo, *J. Catal.* 259 (2008) 133.
- [5] G. Xi, J. Ye, *Catal. Commun.* 46 (2001) 1893.
- [6] S. Navalón, A. Dhkshinamoorthy, M. Alvaro, H. García, *ChemSusChem* 6 (2013) 562.
- [7] L. Zhou, W.Z. Wang, L.S. Zhang, H.L. Xu, W.J. Zhu, *J. Phys. Chem. C* 111 (2007) 13659.
- [8] Y. Zhao, Y. Xie, X. Zhu, S. Yan, S.X. Wang, *Chem. Eur. J.* 14 (2008) 1601.
- [9] H. Jiang, H. Dai, X. Meng, L. Zhang, J. Deng, Y. Liu, C.T.J. Au, *J. Environ. Sci.* 24 (2012) 449.
- [10] H. Jiang, X. Meng, H. Dai, J. Deng, Y. Liu, L. Zhang, Z. Zhao, R. Zhang, *J. Hazard. Mater.* 217–218 (2012) 92.
- [11] A.R. Lim, S.H. Choh, M.S. Jang, *J. Phys.: Condens. Matter* 7 (1995) 7309.
- [12] G. Li, Y. Bai, W.F. Zhang, *Mater. Chem. Phys.* 136 (2012) 930.
- [13] X. Zhang, Z. Ai, F. Jia, L. Zhang, X. Fan, Z. Zou, *Mater. Chem. Phys.* 103 (2007) 162.
- [14] Y. Liu, B. Huang, Y. Dai, X. Zhang, X. Qin, M. Jiang, M.H. Whangbo, *Catal. Commun.* 11 (2009) 210.
- [15] H.M. Zhang, J.B. Liu, H. Wang, W.X. Zhang, H.J. Yan, *Nanoparticles Res.* 10 (2008) 767.
- [16] Y. Park, K.J. McDonald, K.S. Choi, *Chem. Soc. Rev.* 42 (2013) 2321.
- [17] K.E. Kweon, G.S. Hwang, *Phys. Rev. B* 87 (2013) 205202.
- [18] S.J. Hong, S. Lee, J.S. Jang, J.S. Lee, *Energy Environ. Sci.* 4 (2011) 1781.
- [19] W. Yao, H. Iwai, J. Ye, *Dalton Trans.* 11 (2008) 1426.
- [20] M. Long, W. Cai, H. Kisch, *J. Phys. Chem. C* 112 (2008) 548.
- [21] X. Zhang, Y. Gong, X. Dong, X. Zhang, C. Ma, F. Shi, *Mater. Chem. Phys.* 136 (2012) 472.
- [22] N. Murakami, N. Takebe, T. Tsubota, T. Ohno, *J. Hazard. Mater.* 211–212 (2012) 83.
- [23] D. Wang, R. Li, J. Zhu, J. Shi, J. Han, X. Zong, C. Li, *J. Phys. Chem. C* 116 (2012) 5082.
- [24] W.J. Luo, Z.S. Li, T. Yu, Z.G.J. Zou, *J. Phys. Chem. C* 116 (2012) 5076.
- [25] K.P.S. Parmar, H.J. Kang, A. Bist, P. Dua, J.S. Jang, J.S. Lee, *ChemSusChem* 5 (2012) 1926.
- [26] G. Tan, L. Zhang, H. Ren, S. Wei, J. Huang, A. Xia, *ACS Appl. Mater. Interfaces* 5 (2013) 5186.
- [27] H. Fan, T. Jiang, H. Li, D. Wang, L. Wang, J. Zhai, D. He, P. Wang, T. Xie, *J. Phys. Chem. C* 116 (2012) 2425–2430.
- [28] S. Usai, S. Obregón, A.I. Becerro, G. Colón, *J. Phys. Chem. C* 117 (2013) 24479.
- [29] X. Wang, G. Shan, K. Chao, Y. Zhang, R. Liu, L. Feng, Q. Zheng, Y. Sun, Y. Liu, X. Kong, *Mater. Chem. Phys.* 99 (2006) 370.
- [30] S. Obregón, A. Kubacka, M. Fernández-García, G. Colón, *J. Catal.* 299 (2013) 298.
- [31] E.L. Cates, S.L. Chinnapongse, J.H. Kim, J.H. Kim, *Environ. Sci. Technol.* 46 (2012) 12316.
- [32] Y.N. Tang, W.H. Di, X.S. Zhai, R.Y. Yang, W.P. Qin, *ACS Catal.* 3 (2013) 405.
- [33] W. Qin, D. Zhang, D. Zhao, L. Wang, K. Zheng, *Catal. Commun.* 46 (2010) 2304.
- [34] Z.Q. Li, C.L. Li, Y.Y. Mei, L.M. Wang, G.H. Du, Y.J. Xiong, *Nanoscale* 5 (2013) 3030.
- [35] S. Obregón, S.W. Lee, G. Colón, *Dalton Trans.* 43 (2014) 311.
- [36] S. Obregón, G. Colón, *Catal. Commun.* 48 (2012) 7865.
- [37] J. Liu, H. Wang, S. Wang, H. Yan, *Mater. Sci. Eng. B* 104 (2003) 36.
- [38] J. Yu, A. Kudo, *Chem. Lett.* 34 (2005) 850.
- [39] H. Yang, Z. Dai, Z. Sun, *J. Lumin.* 124 (2007) 207.
- [40] N. Zu, H. Yang, Z. Dai, *Physica B* 403 (2008) 174.
- [41] H. Xu, Z. Jiang, *Chem. Phys.* 287 (2003) 155.
- [42] L. Ren, L. Ma, L. Jin, J.B. Wang, M. Qiu, Y. Yu, *Nanotechnology* 20 (2009) 405602.
- [43] S. Obregón, A. Caballero, G. Colón, *Appl. Catal. B: Environ.* 117–118 (2012) 59.
- [44] A. Iwase, A. Kudo, *J. Mater. Chem.* 20 (2010) 7536–7542.
- [45] L. Zhang, J. Long, W. Pan, S. Zhou, J. Zhu, Y. Zhao, X. Wang, G. Cao, *Mater. Chem. Phys.* 136 (2012) 897–902.
- [46] S. Tokunaga, H. Kato, A. Kudo, *Chem. Mater.* 13 (2001) 4624–4628.
- [47] A. Kubacka, G. Colón, M. Fernández-García, *Catal. Today* 143 (2009) 286.